EEET ECOLOGICAL ENGINEERING & ENVIRONMENTAL TECHNOLOGY

Ecological Engineering & Environmental Technology, 2026, 27(10), 490–507
https://doi.org/10.12912/27197050/235854
ISSN 2719–7050, License CC-BY 4.0

Received: 2026.08.01
Accepted: 2026.09.03
Published: 2026.09.10

Short-term hydroclimatic conditions preceding first satellite detection of reconstructed peat-fire events in South Sumatra: An observation-aware case-crossover analysis

Mahturai Rian Fitra[1*], Rujito Agus Suwignyo[2], Dinar Dwi Anugerah Putranto[3], Wijaya Mardiansyah[4]

[1] Doctoral Program in Environmental Science, Graduate School, Universitas Sriwijaya, Jalan Padang Selasa Number 524, Bukit Besar, Palembang 30139, South Sumatra, Indonesia
[2] Department of Agronomy, Faculty of Agriculture, Universitas Sriwijaya, Jalan Raya Palembang-Prabumulih, Kilometer 32, Indralaya, Ogan Ilir 30662, South Sumatra, Indonesia
[3] Master's Program in Civil Engineering, Faculty of Engineering, Universitas Sriwijaya, Jalan Srijaya Negara, Bukit Besar, Palembang 30139, South Sumatra, Indonesia
[4] Department of Physics, Faculty of Mathematics and Natural Sciences, Universitas Sriwijaya, Jalan Raya Palembang-Prabumulih, Kilometer 32, Indralaya, Ogan Ilir 30662, South Sumatra, Indonesia
* Corresponding author's e-mail: rianmahturai@gmail.com

ABSTRACT

The first satellite active-fire detection represents an observation event rather than the timing of ignition. We quantified short-term hydroclimatic conditions preceding the first satellite detection of reconstructed tropical peat-fire events and assessed whether Sentinel-1 C-band backscatter provided information beyond hydroclimatic indicators. We analyzed 79 reconstructed non-singleton MODIS/VIIRS fire events in South Sumatra using a time-stratified case-crossover design comprising 79 case dates and 234 same-weekday referents. CHIRPS rainfall, ERA5-Land vapor pressure deficit (VPD) and soil-water indicators, and Sentinel-1 ΔVV were summarized over prespecified windows spanning 60–1 d before the first retained detection (t0). Conditional logistic regression accounted for satellite observation opportunity on the index date, with uncertainty estimated using 2000 stratum-level bootstrap replicates. The clearest short-term hydroclimatic pattern occurred 1–3 d before t0. An interquartile-range (IQR) increase in VPD was associated with higher case-period odds (odds ratio [OR] 4.07; 95% confidence interval [CI] 1.43–13.54), whereas a wetter rainfall anomaly was associated with lower odds (OR 0.66; 95% CI 0.45–0.86). Lower absolute rainfall and a greater frequency of dry days supported the same drying pattern. Although lag-specific p values did not remain below 0.05 after multiplicity adjustment, shared-bootstrap contrasts indicated stronger standardized associations at 1–3 d than, on average, across longer antecedent windows. Sentinel-1 ΔVV did not materially improve model fit after hydroclimatic adjustment, although earlier-window backscatter changes showed concordance with gridded soil-water conditions. Overall, the findings support a temporally concentrated hydroclimatic drying signal before first satellite detection, without resolving ignition timing. Hydroclimatic indicators provided the clearest near-term information, while Sentinel-1 contributed complementary moisture-sensitive evidence.

Keywords: hydroclimatic conditions, satellite detection, peat fire, South Sumatra, case-crossover, Sentinel-1.

INTRODUCTION

Tropical peat fires arise from interacting controls on peat moisture, atmospheric drying, fuel condition, and ignition opportunity. In drained Indonesian peatlands, groundwater drawdown and reduced peat-water retention progressively limit moisture supply to near-surface peat, increasing its susceptibility to drying and combustion (Taufik et al., 2022; Mezbahuddin et al., 2023). Field evidence from South Sumatra likewise links groundwater conditions with peat-fire occurrence (Irfan et al., 2024), while drainage configuration and land cover further shape spatial fire susceptibility (Salmayenti et al., 2025). Superimposed on these relatively persistent landscape controls are shorter-term atmospheric processes. Vapor pressure deficit (VPD), which represents atmospheric evaporative demand, has emerged as an informative indicator of fire-conducive drying across diverse terrestrial biomes (Clarke et al., 2022; Jain et al., 2022). Recent work in the Himalayas similarly identified VPD as an important control on burned area (Khadke and Ghosh, 2024). Distinguishing these near-term hydroclimatic changes from longer-term landscape susceptibility is therefore important for interpreting the environmental conditions that precede an observable peat-fire signal.

Satellite active-fire products are essential for regional fire monitoring, yet the first recorded detection does not necessarily correspond to the time of ignition. MODIS and VIIRS observe the surface only during discrete satellite overpasses, and active-fire detection can be influenced by cloud or smoke obscuration, viewing geometry, fire intensity, and the temporal evolution of combustion. A fire may therefore already be developing before its first retained satellite detection, while variation in detection timing may partly reflect differences in observation opportunity rather than environmental conditions alone (Chen et al., 2022; McClure et al., 2023). Analyses of pre-detection conditions must consequently distinguish the timing of satellite observation from the underlying – and generally unobserved – timing of ignition.

A related analytical challenge is that a single peat-fire episode may generate multiple active-fire detections across sensors and successive overpasses. In an independently archived event-reconstruction stage, 415 retained MODIS/VIIRS detections were grouped using deterministic 1000-m/24-h graph-based rules, yielding 218 candidate fire events, including 79 non-singleton events supported by at least two retained detections (Fitra et al., 2026a). These event units were defined independently before the hydroclimatic analysis reported here and were carried forward unchanged. Separating event reconstruction from antecedent-condition analysis helps preserve analytical independence and reduces the possibility that event definitions are influenced by the environmental associations subsequently evaluated.

Previous studies have established associations between peat-fire occurrence and seasonal drought, rainfall, groundwater dynamics, and soil moisture (Taufik et al., 2022; Mezbahuddin et al., 2023). Other work has emphasized fire-weather variability and groundwater controls in Indonesian peatlands (Hayasaka, 2023; Irfan et al., 2024), while landscape-scale analyses have shown that drainage density and land cover contribute to persistent spatial fire susceptibility (Salmayenti et al., 2025). Much of this literature, however, has focused on regional fire danger, seasonal variability, or spatial susceptibility. Less is known about whether environmental conditions at a known fire-event location depart from that location's own short-term temporal background immediately before the event becomes detectable by satellite. Evidence at this finer temporal scale remains limited, particularly when reconstructed fire events, hydroclimatic drying, satellite observation opportunity, and radar-based surface-wetness information are evaluated within a common matched framework.

To address this gap, we used a time-stratified case-crossover design adapted to fixed fire-event locations. Each location was compared with itself over time, with the case date matched to same-weekday referent dates within the same month and year. This design controls for time-invariant spatial characteristics and limits confounding by seasonality and longer-term temporal variation, thereby focusing inference on short-term environmental changes preceding detection (Tobias et al., 2024). Within this framework, we examined rainfall, atmospheric evaporative demand, modeled soil-water conditions, and Sentinel-1 backscatter, while explicitly representing active-fire observation opportunity through the availability of valid satellite land observations on case and referent dates.

The study therefore integrates independently reconstructed event units, within-location temporal matching, explicit representation of satellite observation opportunity, and separately quality-controlled Sentinel-1 observations within a single inferential framework. Rather than treating individual hotspots as independent fire events, the analysis evaluates prespecified antecedent windows at fixed event locations while preserving the distinction between environmental conditions and the satellite observation process. Sentinel-1 ΔVV is treated as a complementary moisture-sensitive signal rather than a direct measure of soil moisture because C-band backscatter can also respond to vegetation, surface structure, and acquisition geometry (Quast et al., 2023). Its contribution is therefore assessed in terms of whether it provides information beyond that contained in the hydroclimatic variables.

Accordingly, this study addresses three questions. First, which prespecified antecedent windows, spanning 60 to 1 d before the first retained satellite detection (t0), show the clearest evidence of short-term hydroclimatic change? Second, does Sentinel-1 ΔVV provide additional information beyond rainfall, VPD, and near-surface soil-water conditions? Third, how robust are these associations to alternative representations of satellite observation opportunity, radar windows and baselines, prior-event restrictions, and year-level influence? Supporting analyses further examine absolute rainfall accumulation, dry-day frequency, deeper ERA5-Land soil-water conditions, and Sentinel-1–hydroclimate wetness concordance. Throughout the study, t0 refers specifically to the first retained satellite active-fire detection and is not interpreted as the time of ignition.

MATERIALS AND METHODS

Study area and spatial framework

The study was conducted in the Tanjung Lago–Banyuasin II peatland landscape in the lower Musi River delta, South Sumatra, Indonesia. The study area encompassed peat polygon GID 155, covering approximately 142.35 km². Under the Indonesian semi-detailed peat-mapping scheme, the polygon is classified as D2 peat, corresponding to a mapped peat-depth class of ≥100 to <200 cm (Anda et al., 2021). This classification was used only to characterize the broader peatland setting and should not be interpreted as a field-validated estimate of peat depth at individual fire-event locations.

All distance- and buffer-based spatial analyses were performed in WGS 84 / UTM Zone 48S (EPSG:32748), whereas geographic coordinates were retained in WGS 84 (EPSG:4326) for data exchange, reporting, and reproducibility. Figure 1 shows the regional setting and the active-fire detection archive used in the independent event-reconstruction stage, which yielded 218 candidate fire events. The primary analysis was

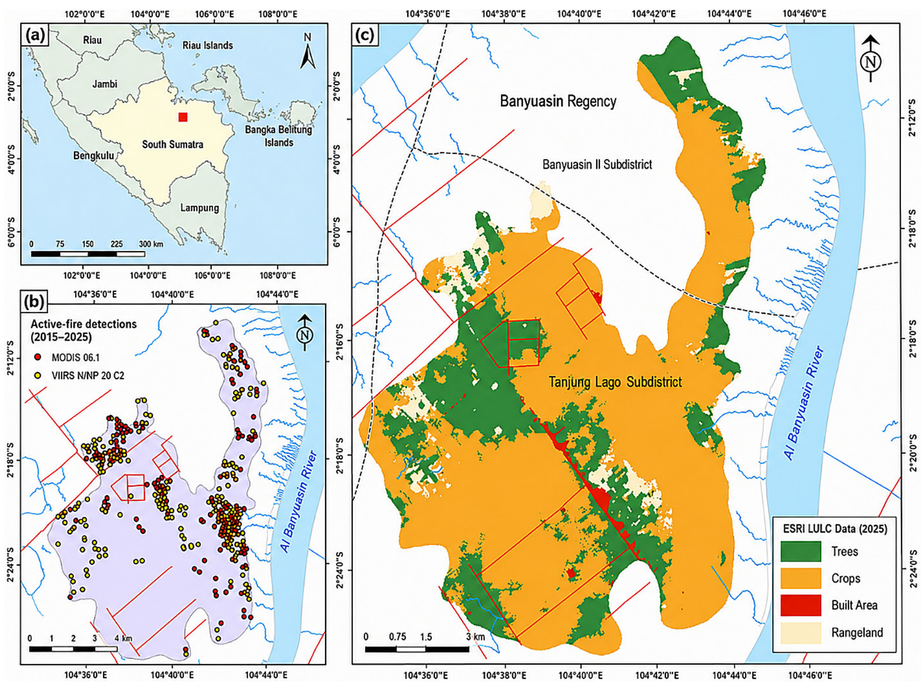

Figure 1. Study-area context of the Tanjung Lago–Banyuasin II peatland landscape, South Sumatra, Indonesia: (a) regional location; (b) confidence-filtered MODIS/VIIRS active-fire detections used in the independent reconstruction of candidate fire events; and (c) land-cover and local landscape setting. The present analysis included 79 non-singleton reconstructed fire events derived from this inventory (Fitra et al., 2026a). Individual active-fire detections are shown for spatial context only and were not treated as independent analytical events

restricted to the 79 non-singleton reconstructed events supported by at least two retained detections. Individual active-fire detections shown in Figure 1 are provided for spatial context and were not treated as independent fire events in the present analysis.

Response inventory and analysis populations

The response inventory was derived from the preceding event-reconstruction stage rather than generated de novo for the present analysis (Fitra et al., 2026a). In that stage, 415 retained MODIS/VIIRS active-fire detections were consolidated into 218 candidate fire events using prespecified deterministic graph-based rules. The inventory covered the period from 22 February 2015 to 29 October 2025 and comprised 34 multi-product clusters, 45 single-product non-singleton clusters, and 139 singletons.

Event membership, identifiers, centroids, provenance fields, chain flags, and the timing of the first retained detection (*t0*) were carried forward unchanged. No event was added, merged, removed, or reclassified on the basis of hydroclimatic exposures, Sentinel-1 variables, or subsequent statistical results. The 79 non-singleton events constituted the primary inferential population, whereas the full inventory of 218 candidate events was retained for provenance tracking and prior-event auditing. This separation maintained a clear analytical boundary between event reconstruction and subsequent inference on antecedent environmental conditions.

The response inventory began on 22 February 2015. Referent dates were generated deterministically using the same-weekday matching rule and retained when the required environmental-exposure and observation-opportunity data were available. In the earliest matched stratum, some referent dates preceded the start of the response inventory. These dates were used solely as temporal comparison periods and were not interpreted as evidence of an absence of fire activity. Specifically, the referent dates of 1, 8, and 15 February 2015 in STR_C0001 occurred before the inventory start date. Because fire-event history before 22 February 2015 could not be assessed from the available response inventory, this archive-edge condition was evaluated separately in a post hoc sensitivity analysis.

Outcome definition and observation opportunity

The case date was defined as the local calendar date containing *t0*, the first retained satellite active-fire detection associated with an eligible reconstructed fire event. This date represented the timing of first satellite observation and was not interpreted as the date or time of ignition. All retained active-fire timestamps were converted from Coordinated Universal Time (UTC) to Western Indonesia Time (WIB; UTC+7) before case dates were assigned. Accordingly, all antecedent exposure windows represented environmental conditions preceding the first retained satellite observation of an active-fire signal.

Active-fire observation opportunity was assessed independently for each case and referent date using Terra MODIS MOD14A1, Aqua MODIS MYD14A1, and Suomi-NPP VIIRS VNP14A1 FireMask products within a 1000-m buffer around each event centroid (Giglio et al., 2016; Schroeder et al., 2014). FireMask class 5 (non-fire land) and classes 7–9 (fire detections of low, nominal, and high confidence) were treated as valid local land observations, whereas cloud, unknown, missing, and unprocessed classes were treated as invalid for observation-opportunity assessment. A sensor was classified as valid on a given local index date when at least one valid-land pixel occurred within the 1000-m event buffer. The primary observation-opportunity covariate, *n_valid_sensors*, was defined as the number of the three satellite sensors satisfying this criterion and therefore ranged from 0 to 3.

This covariate was intended to capture the opportunity for an active-fire signal to be observed rather than the physical intensity of the fire. Because *n_valid_sensors* was derived from the same active-fire product family used to define *t0*, it was treated as an ascertainment-process covariate rather than as an independent environmental exposure. Fire counts, detection-confidence scores, and fire radiative power were therefore excluded from the environmental predictor set to avoid introducing outcome-derived information into models designed to evaluate antecedent environmental conditions.

Referent-date selection

A time-stratified case-crossover design was used to compare each fire-event location with itself across nearby referent periods. For each case date, all other dates within the same month and year that fell on the same day of the week were selected as referent dates. Referent selection was deterministic rather than random, yielding one case date and two to four referent dates within each retained stratum.

The history of earlier candidate fire events was evaluated separately through a prespecified prior-event audit. This audit served as an additional quality-control procedure and did not alter the original referent-selection rule or retrospectively modify matched sets after exposure extraction.

Matching on day of the week within the same month and year helps control for seasonality, longer-term temporal trends, and systematic weekly patterns, consistent with current methodological guidance for time-stratified case-crossover analyses of short-term environmental exposures (Tobias et al., 2024). Primary hydroclimatic exposures were summarized using prespecified, mutually exclusive antecedent lag blocks to reduce redundancy among adjacent lag metrics and maintain clear temporal interpretation. Because case and referent dates within a stratum can occur relatively close in time, some temporal dependence among their exposure summaries was expected. This dependence was considered when interpreting the precision, stability, and uncertainty of the estimated associations rather than assuming that matched exposure summaries were temporally independent.

Data sources and spatial extraction

Hydroclimatic conditions were characterized using ERA5-Land Hourly data and CHIRPS Daily precipitation. From ERA5-Land, we extracted 2-m air temperature, 2-m dew-point temperature, volumetric soil water in layer 1 (SWVL1; 0–7 cm), and volumetric soil water in layer 2 (SWVL2; 7–28 cm). Daily mean vapor pressure deficit (VPD) and daily mean SWVL1 were prespecified as the primary ERA5-Land indicators, whereas maximum VPD, SWVL2, and other derived hydroclimatic indicators were retained for supporting analyses (Muñoz-Sabater et al., 2021).

CHIRPS Daily precipitation was used to derive antecedent rainfall accumulation, rainfall anomalies, wet-day frequency, and consecutive dry-day metrics (Funk et al., 2015). The reconstructed event inventory provided the spatial and temporal anchors for environmental extraction, primarily the event centroid and *t0*, together with provenance information including cluster type, detection count, sensor provenance, chain flags, and Sentinel-1 evidence status. MODIS and VIIRS FireMask products and their associated quality information were analyzed separately to characterize satellite observation opportunity on case and referent dates; they were not included as additional fire-response variables.

Sentinel-1 ground range detected (GRD) observations acquired in interferometric wide swath (IW) mode with VV and VH polarizations were used to characterize antecedent backscatter changes. ΔVV was prespecified as the primary radar metric, while additional polarization information was retained for supporting and wetness-concordance analyses. The primary reference period, B120, covered days 61–120 before each case or referent index date, whereas B90 (days 61–90) served as an alternative baseline for sensitivity analysis. Three antecedent radar windows were prespecified: W1 (days 31–60), W2 (days 15–30), and W3 (days 1–14).

Only Sentinel-1 acquisitions obtained before the corresponding index date were eligible for analysis, preventing post-index observations from contributing to estimates of antecedent conditions. Orbit direction and relative orbit were held consistent within the corresponding case–referent comparisons to reduce variability attributable to acquisition geometry (Torres et al., 2012; Mullissa et al., 2021).

CHIRPS rainfall was summarized as the spatial mean within a 1000-m buffer around each event centroid. Because the native CHIRPS grid (0.05°) is substantially coarser than the extraction buffer, these summaries were interpreted as gridded representations of broader rainfall conditions surrounding each event location rather than as precipitation estimates resolved at the 1-km scale. Sentinel-1 backscatter was summarized separately within a prespecified 500-m buffer around each event centroid. This buffer defined the spatial support for radar aggregation and should not be interpreted as the native spatial resolution of the Sentinel-1 observations. ERA5-Land variables were likewise treated as gridded indicators of the broader hydroclimatic environment rather than as site-specific field measurements. Accordingly, neither CHIRPS nor ERA5-Land was used to infer environmental variability below the spatial resolution of the underlying gridded products. The principal data streams and their analytical roles are summarized in Table 1.

Time alignment and exposure construction

ERA5-Land hourly observations were first aligned to local calendar days in Western Indonesia Time (WIB; UTC+7). Air temperature (T) and dew-point temperature (T_d) were converted from Kelvin to degrees Celsius before vapor-pressure calculations. Hourly vapor pressure deficit (VPD) was calculated as

$$VPD = max[e_s(T) - e_a(T_d), 0] \quad (1)$$

where: $e_s(T)$ denotes saturation vapor pressure at the 2-m air temperature and $e_a(T_d)$ denotes actual vapor pressure estimated from the 2-m dew-point temperature.

Vapor pressures were calculated as $e_s(T) = 0.6108 \exp[17.27T/(T + 237.3)]$ and $e_a(T_d) = 0.6108 \exp[17.27T_d/(T_d + 237.3)]$, with temperature expressed in °C and vapor pressure in kPa. Daily mean VPD was prespecified as the primary indicator of atmospheric evaporative demand, whereas daily maximum VPD was retained for sensitivity analysis. ERA5-Land volumetric soil water in layers 1 and 2 (SWVL1 and SWVL2) was averaged over the same local calendar days. Daily ERA5-Land summaries were retained only when all 24 hourly observations were available; missing hourly values were not imputed.

Environmental exposures were summarized over five prespecified, mutually exclusive antecedent periods relative to each case or referent index date: days 1–3, 4–7, 8–14, 15–30, and 31–60. Lag 0 was excluded to ensure that all exposure summaries represented conditions preceding, rather than occurring on, the index date. These lag blocks were defined before final statistical modeling and were not selected on the basis of observed associations.

For CHIRPS, daily rainfall anomalies were calculated as observed precipitation minus the corresponding 1991–2020 climatological mean for each calendar day. The climatology was derived from the same CHIRPS product and spatial extraction procedure used to construct the event-level rainfall series. Daily anomalies were then summed within each antecedent lag block to obtain cumulative rainfall departure, expressed in millimeters. ERA5-Land VPD, SWVL1, and SWVL2 were summarized over the corresponding lag blocks as arithmetic means. Missing environmental values were not imputed, and a lag-specific exposure summary was retained only when the prespecified completeness criterion for that block was satisfied.

Construction of the Sentinel-1 surface-wetness proxy

Sentinel-1 GRD IW observations were restricted to scenes containing both VV and VH polarizations, adequate coverage of the 500-m event buffer, and a consistent orbit direction and relative orbit within each matched stratum. The high-resolution GRD product with 10 × 10 m pixel spacing was used. A single eligible orbit configuration was retained across each case and its referents, and acquisitions on or after the index date were excluded so that all radar metrics preceded the first retained active-fire detection (*t0*).

The primary baseline, B120, covered days 61–120 before the index date; B90 (61–90 d) was reserved for sensitivity analysis. Three mutually exclusive antecedent windows were evaluated: W1 (31–60 d), W2 (15–30 d), and W3 (1–14 d). Median VV and VH backscatter were summarized within each period. The primary radar metric, ΔVV, was defined as the median VV backscatter in each recent window minus the corresponding B120 median, while ΔVH and polarization-based metrics were retained as supporting measures.

Radar quality-control criteria were prespecified and fixed. A valid comparison required at least two unique B120 acquisitions, at least one acquisition within the target window, a valid-pixel fraction of at least 0.60 and a consistent orbit configuration within the stratum. The valid-pixel

Table 1. Environmental data streams and analytical roles

Data source	Principal variables / analytical role
CHIRPS Daily	Rainfall accumulation, anomaly, wet-day and dry-day metrics
ERA5-Land	VPD; SWVL1 (0–7 cm); SWVL2 (7–28 cm)
Sentinel-1 GRD IW	ΔVV relative to B120 as a moisture-sensitive surface-wetness proxy
MODIS/VIIRS	First active-fire detection outcome and observation opportunity
Reconstructed event inventory	Event t0, centroid, provenance, chain flags, and prior-event audit

fraction was calculated within the 500-m buffer from the joint VV-and-VH composite mask at 10-m processing scale, with valid pixels requiring both polarizations to be unmasked. Missing radar observations were not imputed. W1–W3 were analyzed separately, and a stratum contributed to a window-specific model only when the case and at least two referents satisfied both baseline and window-specific quality-control criteria.

Pilot extraction, protocol freezing, and batch strategy

A multiwindow pilot extraction was conducted on ten strata to finalize the Sentinel-1 processing protocol before full analysis. Extending the baseline from B90 to B120 substantially improved baseline data completeness; therefore, B120 was prespecified as the primary baseline, while B90 was retained for sensitivity analysis. This decision was based solely on data availability and was made before evaluating the magnitude or direction of exposure–outcome associations.

After the protocol was frozen, the 79 non-singleton events were processed in 16 predefined batches using an identical three-stage workflow: orbit selection, baseline extraction, and extraction of the W1–W3 antecedent windows. Batch outputs were subsequently consolidated into a single analysis dataset before inferential modeling.

Primary radar exposure and hypothesis framework

Sentinel-1 metrics were analyzed separately for each antecedent window to preserve their temporal interpretation and limit model complexity. ΔVV relative to the B120 baseline was prespecified as the primary radar metric, while ΔVH, polarization-based metrics, and radar vegetation indices were retained as supporting measures. W1 (31–60 d) was used for primary integration with hydroclimatic variables because it retained the largest quality-controlled matched sample, rather than because of the magnitude or direction of its estimated association.

The analysis allowed drying-related signals to occur at different antecedent time scales: W1 represented earlier conditions, W2 (15–30 d) intermediate conditions, and W3 (1–14 d) conditions closest to *t0*. The direction of ΔVV was not assigned a priori to drying or wetting. Instead, radar changes were interpreted as moisture-sensitive evidence only when supported by independent hydroclimatic indicators and consistent across prespecified sensitivity analyses (Hrysiewicz et al., 2023).

Descriptive analysis and event-study visualization

Sample flow was documented from the 218 reconstructed events to the 79-event primary population and the window-specific Sentinel-1 subsets. Data completeness was summarized using acquisition counts, valid-pixel fractions, daily exposure completeness, and active-fire observation opportunity. A common observation identifier maintained linkage across all data sources and audit variables.

Pre-detection plots visualized within-stratum case–referent differences from 60 to 1 d before *t0*. Sentinel-1 values were shown only on actual acquisition dates, with no interpolation between observations, while radar windows were summarized as recent-minus-baseline contrasts. For CHIRPS, daily rainfall-anomaly differences were calculated as the case value minus the mean of the corresponding referent values.

Uncertainty bands were estimated from 2000 bootstrap replicates by resampling entire strata, thereby preserving the matched structure. These plots were descriptive and were not used to select exposure windows or hypotheses based on lag-specific statistical significance.

Primary inferential models

Because VPD and SWVL1 were strongly inversely correlated within matched strata, they were evaluated in separate primary models to limit collinearity and preserve interpretability. H-VPD included rainfall anomaly, mean VPD, and *n_valid_sensors*, whereas H-SW included rainfall anomaly, mean SWVL1, and *n_valid_sensors*. A joint H-FULL model containing both VPD and SWVL1 was retained only as a sensitivity analysis.

H-VPD and H-SW were fitted separately for each prespecified lag block using conditional logistic regression stratified by *stratum_id_model*. Hydroclimatic associations were expressed per interquartile-range (IQR) increase, with scaling constants fixed from the primary analysis sample; *n_valid_sensors* was expressed per additional sensor providing a valid land observation. For Sentinel-1 integration, W1 was paired with the corresponding 31–60-d hydroclimatic window. Hydroclimatic models were first refitted on the W1-eligible sample before ΔVV was added, ensuring that likelihood-ratio tests and Akaike information criterion (AIC) comparisons used identical observations.

One interaction between centered, IQR-scaled VPD and ΔVV was prespecified for W1, with both main effects retained. No additional interactions, lag windows, or radar metrics were promoted to primary analyses after examination of the results.

Association interpretation and uncertainty

The analysis estimated relative associations rather than ignition thresholds or operational warning cut-offs. Results were therefore reported as odds ratios with 95% confidence intervals and interpreted according to association magnitude, direction, timing, and consistency across prespecified analyses.

Model-based confidence intervals were complemented by percentile intervals from 2000 bootstrap replicates in which entire matched strata were resampled to preserve the case-crossover structure. IQR scaling was fixed from the primary analysis sample, and a prespecified random seed (20260809) was used for reproducibility. Nonconvergent bootstrap fits were excluded from percentile-interval estimation but recorded in the analysis audit. Bootstrap intervals and model-based p values were retained as distinct uncertainty summaries; because they rely on different inferential approximations, occasional disagreement was interpreted as uncertainty rather than resolved by selecting the more favorable result. Interpretation emphasized association magnitude, interval width, temporal coherence, and robustness across sensitivity analyses rather than statistical significance alone.

Sensitivity and robustness analyses

Prespecified sensitivity analyses evaluated robustness to radar timing, baseline definition, prior-event history, observation opportunity, hydroclimatic collinearity, and year-level influence. Sentinel-1 temporal sensitivity was assessed using quality-control-eligible W2/B120 and W3/B120 samples paired with the corresponding 15–30-d and 1–14-d hydroclimatic windows. Baseline sensitivity replaced B120 with B90 while retaining W1 and the 31–60-d hydroclimatic window.

Potential influence from earlier reconstructed events was examined by excluding matched observations with a candidate-event onset within 1 km and 1–120 d before the index date. Observation-opportunity sensitivity compared the primary *n_valid_sensors* adjustment with unadjusted models and models using mean valid-land fraction. Hydroclimatic collinearity was assessed using H-FULL, which jointly included rainfall anomaly, VPD, SWVL1, and *n_valid_sensors*.

For each eligible sample, the incremental contribution of Sentinel-1 ΔVV was assessed against the corresponding hydroclimatic model fitted to identical observations using likelihood-ratio tests and AIC. Major sensitivity models retained 2000-replicate stratum-level bootstrap intervals. These analyses assessed robustness and did not alter the prespecified primary temporal window.

Year-level influence was evaluated by refitting the L1–3 H-VPD and H-SW models after excluding each contributing year in turn. IQR scaling from the primary analysis sample was retained for comparability. Interpretation emphasized stability in association direction and magnitude rather than statistical significance in the reduced samples.

After completion of the prespecified analyses, three additional post hoc robustness diagnostics were conducted without altering the primary models. First, referent dates with n_valid_sensors = 0 were excluded and the 1–3-d H-VPD and H-SW models were refitted; a stricter analysis retained only strata with at least two eligible referents after this exclusion. Second, the entire earliest stratum (STR_C0001) was excluded because its three deterministic February 2015 referents preceded the start of the upstream response inventory. For both exclusion analyses, primary-sample IQR scaling and the 2000-replicate stratum-level bootstrap were retained. Third, because five hydroclimatic lag blocks were evaluated in parallel, model-based p-values within each primary exposure family were adjusted using Benjamini–Hochberg and Holm procedures. Temporal concentration was additionally assessed using 2000 shared stratum-level bootstrap resamples by contrasting the standardized log-odds ratio for 1–3 d with the mean standardized log-odds ratio across the four longer lag blocks. These diagnostics were interpreted as robustness checks rather than as prespecified confirmatory tests. The complete analysis workflow is summarized in Figure 2.

Supporting hydrological analyses

Supporting analyses examined rainfall availability and deeper soil-water conditions without modifying the primary hydroclimatic models. ERA5-Land SWVL2 (7–28 cm) was evaluated using a model parallel to H-SW, including rainfall anomaly, SWVL2, and *n_valid_sensors* for each prespecified lag block.

Absolute CHIRPS rainfall accumulation, dry-day frequency (<1 mm d^{-1}), and consecutive dry days ending at lag 1 were evaluated separately as complementary indicators of rainfall availability. Continuous associations were expressed per IQR increase using scaling fixed from the primary analysis sample, with uncertainty estimated from 2000 stratum-level bootstrap replicates. SWVL2 and related hydrological metrics were interpreted as gridded environmental indicators rather than direct field measurements of peat water-table conditions.

Sentinel-1-hydroclimate wetness concordance

A complementary analysis evaluated whether Sentinel-1 ΔVV varied consistently with independent hydroclimatic indicators. W1, W2, and W3 were paired with the corresponding 31–60-d, 15–30-d, and 1–14-d hydroclimatic windows, respectively.

Within each stratum, case-minus-mean-referent contrasts were calculated for ΔVV, rainfall anomaly, VPD, and SWVL1. Pearson correlations were estimated with 95% intervals from 2000 stratum-level bootstrap replicates, while Spearman and pooled within-stratum-centered correlations were used as sensitivity analyses. This analysis assessed cross-variable consistency in moisture-related signals rather than converting Sentinel-1 backscatter into estimates of absolute soil moisture.

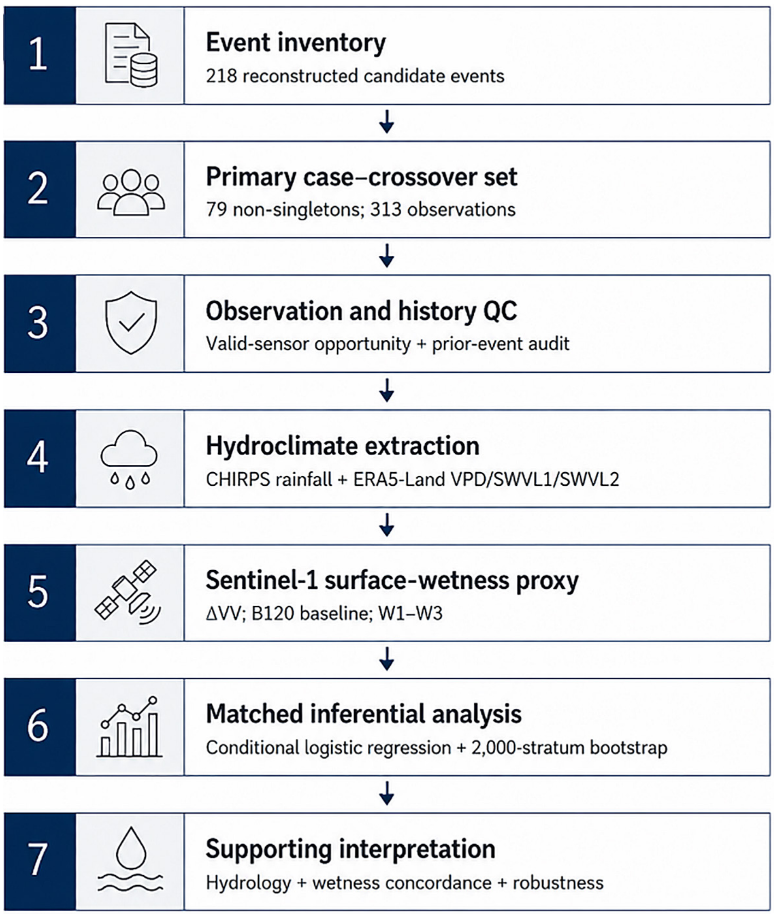

Figure 2. Reproducible analysis workflow linking the reconstructed MODIS/VIIRS event inventory with the time-stratified case-crossover design, observation-opportunity and prior-event quality control, Sentinel-1 multi-window extraction, CHIRPS rainfall and 1991–2020 climatology, hydroclimatic modeling, and prespecified sensitivity and robustness analyses

Reproducibility and protocol freezing

Key analytical decisions – including population definitions, referent selection, spatial buffers, time alignment, exposure construction, Sentinel-1 baselines and windows, quality-control criteria, and model specifications – were fixed before final inferential modeling and remained unchanged thereafter.

Supporting hydrological and Sentinel-1–hydroclimate concordance analyses were conducted without altering the predefined primary analysis sequence. Stable observation identifiers maintained traceability across event records, environmental exposures, audit variables, and model inputs.

As an additional integrity check, the final analytical dataset was independently reconstructed from archived case–referent keys and the original data sources using the frozen spatial, temporal, and quality-control rules. Completeness, duplicate keys, exposure windows, and model inputs were re-audited before final reruns. Archived outputs served only as consistency benchmarks; discrepancies were documented rather than resolved by modifying event definitions, exposure values, or analytical rules. A final portability audit reran the archived Python workflow from the integrated analytical dataset and reproduced the critical tabular model outputs and figure-source tables exactly.

RESULTS

The primary analysis included 313 observations from 79 matched strata: 79 case observations and 234 referents. CHIRPS, ERA5-Land, observation-opportunity, and event-history variables were complete for all observations, whereas Sentinel-1 availability varied across antecedent windows according to the prespecified quality-control criteria.

Data completeness and observation opportunity

ERA5-Land and CHIRPS exposures were complete across the full 60-d pre-index period for all 313 observations, representing 18,780 observation-days. The reproducibility audit confirmed one-to-one linkage across analytical records, with no duplicate keys or missing required hydroclimatic exposures. All prespecified variables needed for the integrated analysis were successfully reconstructed, and reruns preserved the direction and temporal pattern of the principal hydroclimatic associations.

Active-fire observation opportunity ranged from zero to three valid sensors on matched index dates. All 79 case dates had at least one valid active-fire observation on *t0*. Events were temporally concentrated, with 49 of 79 events occurring in 2015 and 14 in 2019; the remaining contributing years contained one to five events each. This concentration motivated the prespecified leave-one-year-out influence analysis.

Hydroclimatic associations across prespecified lag blocks

The clearest hydroclimatic associations occurred during the final 1–3 d before t0. In the H-VPD model, an IQR increase in mean VPD (0.880 kPa) was associated with substantially higher case-period odds (OR 4.07; bootstrap 95% CI 1.43–13.54; model-based $p = 0.021$). Associations at longer antecedent windows were weaker and less precisely estimated, indicating that the atmospheric-drying signal was concentrated close to first satellite detection.

Rainfall showed a corresponding short-term pattern. In the H-SW model, an IQR increase in rainfall anomaly toward wetter conditions (10.97 mm) was associated with lower case-period odds at 1–3 d (OR 0.66; bootstrap 95% CI 0.45–0.86; model-based $p = 0.024$). The rainfall estimate in H-VPD had the same direction but greater uncertainty. SWVL1 also yielded an OR below 1, although its bootstrap interval was wide (OR 0.48; 95% CI 0.14–1.55). Thus, the short-term rainfall and atmospheric-demand signals were more clearly resolved than the association with gridded near-surface soil water.

Observation opportunity was independently associated with case status. In the 1–3-d H-VPD model, each additional active-fire sensor providing a valid land observation was associated with higher case-period odds (OR 2.36; bootstrap 95% CI 1.48–4.68). Because the outcome was defined by first satellite detection, this association was interpreted as evidence of the observation process rather than as a physical driver of peat-fire occurrence. The lag-specific hydroclimatic estimates are summarized in Figure 3.

Sentinel-1-only and hydroclimate-integrated models

Sentinel-1-only associations were weak across the three prespecified antecedent windows. Relative to the B120 baseline, ΔVV yielded odds ratios per IQR of 1.16 for W1, 1.10 for W2, and 0.95 for W3, with no clear temporal pattern. After hydroclimatic adjustment in the W1-eligible sample (78 strata; 307 observations), ΔVV remained close to the null in H-VPD+S1 (OR 1.02; bootstrap 95% CI 0.52–2.22) and was similarly imprecise in H-SW+S1 (OR 1.17; 0.59–2.59). Adding ΔVV did not improve model fit in H-VPD (likelihood-ratio $p = 0.949$; ΔAIC = +2.00). The prespecified VPD × ΔVV interaction was also imprecisely estimated, providing little evidence that the association between antecedent atmospheric drying and first satellite detection varied systematically with the Sentinel-1 backscatter signal. Adjusted ΔVV estimates and the principal radar sensitivity results are shown in Figure 4.

Robustness and sensitivity analyses

Sentinel-1 showed no consistent evidence of incremental information across the prespecified sensitivity analyses. After H-VPD adjustment, ΔVV odds ratios were 1.15 (bootstrap 95% CI 0.70–1.84) for W2/B120, 0.95 (0.49–1.69) for W3/B120, 0.99 (0.54–2.94) for W1/B90, and 1.48 (0.47–4.33) in the prior-event-clean W1 subset. The corresponding H-SW models supported the same interpretation. Across analyses, adding ΔVV did not materially improve fit by either AIC or nested likelihood-ratio comparison.

The short-term hydroclimatic pattern was also stable under alternative representations of observation opportunity. Without adjustment for observation opportunity, VPD at lag 1–3 d remained positively associated with first satellite detection (OR 4.03; bootstrap 95% CI 1.38–12.80), while rainfall anomaly in H-SW remained inversely associated (OR 0.62; 0.42–0.79). Replacing the sensor-count adjustment with the mean valid-land

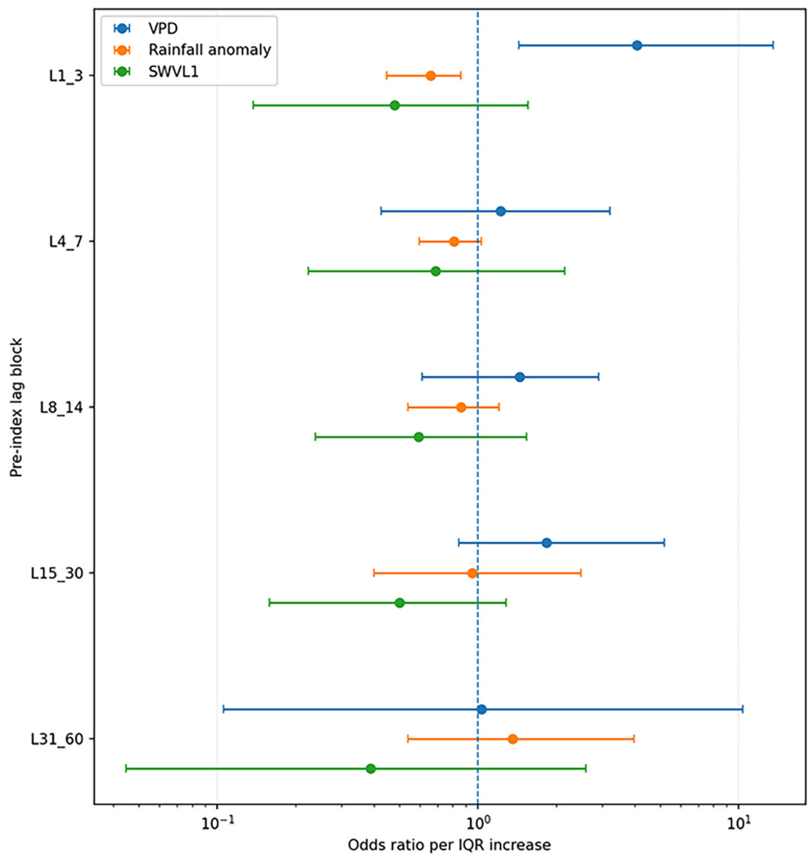

Figure 3. Hydroclimatic associations preceding the first satellite active-fire detection
Note: Odds ratios (ORs) per interquartile-range (IQR) increase are shown for mean vapor pressure deficit (VPD; H-VPD), rainfall anomaly (H-SW), and ERA5-Land surface soil water in layer 1 (SWVL1; H-SW) across the five prespecified lag blocks. Points represent estimated ORs, and error bars indicate 95% bootstrap percentile intervals based on 2000 stratum-level resamples

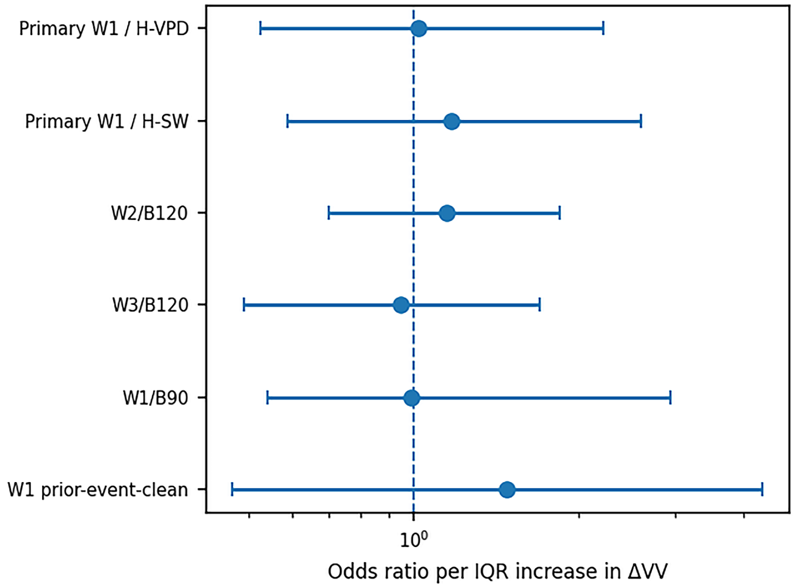

Figure 4. Sentinel-1 ΔVV associations after hydroclimatic adjustment
Note: Primary W1 estimates are shown for the H-VPD and H-SW models, followed by H-VPD-adjusted sensitivity estimates for W2/B120, W3/B120, the alternative W1/B90 baseline, and the prior-event-clean W1 subset. Error bars represent 95% percentile intervals from 2000 stratum-level bootstrap replicates

fraction produced similar estimates for VPD (OR 4.06; 1.39–13.35) and rainfall anomaly (OR 0.65; 0.45–0.85). In contrast, the joint H-FULL model showed marked coefficient instability, including changes in magnitude and direction when VPD and SWVL1 were entered together. This pattern was consistent with the strong within-stratum collinearity identified before model fitting.

Ten of 234 referent observations had n_valid_sensors = 0, whereas none of the 79 case observations had zero observation opportunity. Excluding these referents retained all 79 strata (303 observations) and did not materially alter the primary short-term associations: VPD remained strongly positive in H-VPD (OR 4.18; bootstrap 95% CI 1.47–14.17) and rainfall anomaly remained inverse in H-SW (OR 0.65; 0.44–0.86). A stricter analysis retaining at least two eligible referents per case yielded similar estimates (75 strata; VPD OR 3.89, 95% CI 1.31–12.89; rainfall anomaly OR 0.66, 95% CI 0.44–0.88). A separate archive-edge sensitivity excluded STR_C0001, the only matched stratum with referent dates preceding the upstream response-inventory start. The reduced sample retained 78 strata (309 observations) and preserved the primary short-term pattern (VPD OR 4.29; bootstrap 95% CI 1.47–14.39; H-SW rainfall anomaly OR 0.66; 0.45–0.88).

As a post hoc multiplicity diagnostic, the 1–3-d VPD and rainfall-anomaly estimates had the smallest model-based p-values within their respective five-lag families, although neither remained below 0.05 after Benjamini–Hochberg or Holm adjustment (VPD: raw $p = 0.021$, adjusted $p = 0.104$; rainfall anomaly: raw $p = 0.024$, adjusted $p = 0.119$). Shared-bootstrap contrasts nevertheless indicated stronger standardized associations at 1–3 d than, on average, across the four longer lag blocks (VPD ratio of ORs 3.01, bootstrap 95% CI 1.06–9.18; rainfall-anomaly ratio of ORs 0.67, 0.41–0.99). These diagnostics support a temporally concentrated pattern while cautioning against interpretation based on isolated lag-specific p-values. The daily rainfall-anomaly contrasts are shown descriptively in Figure 5.

The year-level influence analysis did not change the direction of either primary short-term association. Across leave-one-year-out refits, the VPD odds ratio at 1–3 d ranged from 3.02 to 5.60 and remained above 1, while the H-SW rainfall-anomaly odds ratio ranged from 0.55 to 0.75 and remained below 1. Excluding 2015, which contributed 49 of the 79 primary events, reduced the analysis to 30 strata and, as expected, increased uncertainty; nevertheless, the point estimates retained the same direction (VPD OR 4.64; rainfall anomaly OR 0.75). The short-term pattern was therefore not driven solely by any single year, although the strong concentration of events in 2015 remains an important limitation for precision and generalizability.

Supporting hydrological-condition analysis

The supporting hydrological analysis provided complementary evidence of reduced water input immediately before first satellite detection. At 1–3 d, an IQR increase in observed rainfall accumulation (19.05 mm) was associated with lower case-period odds (OR 0.42; bootstrap 95% CI 0.22–0.65), whereas an IQR increase of two dry days (<1 mm d^{-1}) was associated with higher odds (OR 2.29; 1.26–4.56). SWVL2 at the same lag yielded an OR below 1, although the estimate was imprecise (OR 0.81; 0.29–2.12). Longer-window SWVL2 estimates were broadly similar in direction but remained uncertain.

At 31–60 d, the dry-day estimate was elevated (OR 2.91; bootstrap 95% CI 1.10–8.41), whereas the corresponding model-based p value was 0.073. Because the bootstrap percentile interval and model-based test yielded different inferential signals, and because this was a supporting analysis, the estimate was treated as unstable and suggestive rather than confirmatory. Consecutive dry days immediately preceding lag 1 were also imprecisely estimated (OR 1.30; bootstrap 95% CI 0.95–2.11). Selected supporting hydrological estimates are summarized in Figure 6.

Sentinel-1-hydroclimate wetness concordance

Sentinel-1 ΔVV was positively correlated with SWVL1 at W1 (r = 0.34; bootstrap 95% CI 0.14–0.53) and W2 (r = 0.36; 0.13–0.57). At W2, ΔVV was also inversely correlated with VPD (r = -0.31; bootstrap 95% CI -0.55 to -0.06), whereas the corresponding W1 correlation was weak. At W3, correlations of ΔVV with both SWVL1 and VPD were close to zero and imprecisely estimated. Relationships with rainfall anomaly were less consistent across windows.

When variables were centered within strata and then pooled, the positive ΔVV–SWVL1 relationships at W1 and W2 remained evident. Together, these patterns are consistent with the expected moisture sensitivity of Sentinel-1 backscatter, but they do not establish ΔVV as a direct or quantitative measure of soil moisture. Window-specific wetness-concordance estimates are shown in Figure 7.

Taken together, the primary and supporting analyses indicate a concentrated short-term drying pattern immediately before first satellite detection. Atmospheric evaporative demand was higher, rainfall was below climatological expectation, total rainfall input was reduced, and dry days were more frequent. Gridded soil-water indicators were broadly consistent with this pattern, although less precisely estimated. Sentinel-1 ΔVV also showed moisture-sensitive relationships during the 15–60 d antecedent period, but provided little evidence of incremental information beyond hydroclimatic conditions and variation in satellite observation opportunity. Selected primary and supporting estimates are summarized in Table 2.

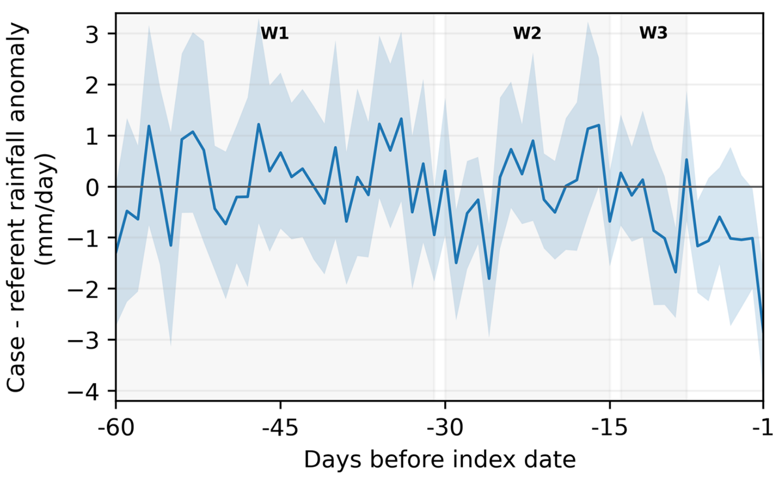

Figure 5. Descriptive event-study of daily CHIRPS rainfall anomalies before first satellite detection
Note: The solid line shows the mean within-stratum difference between case and referent rainfall anomalies at each lag from 60 to 1 d before the index date, while the shaded band represents the corresponding stratum-level bootstrap interval. The figure is intended to illustrate the temporal pattern of rainfall conditions and was not used to define or select the prespecified lag blocks

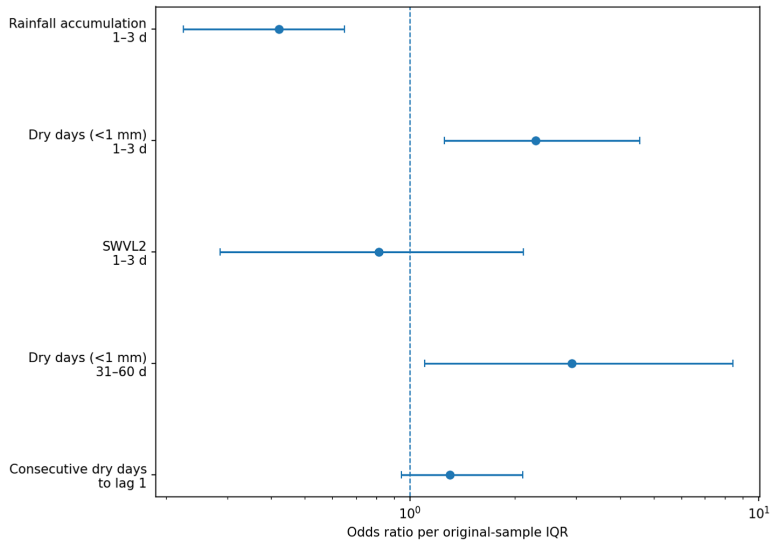

Figure 6. Supporting hydrological-condition associations before first satellite active-fire detection
Note: Odds ratios are expressed per interquartile-range (IQR) increase based on the original analysis sample, with error bars representing 95% percentile intervals from 2000 stratum-level bootstrap replicates. SWVL2 represents gridded soil-water conditions at 7–28 cm depth and should not be interpreted as a direct measurement of peat water-table depth

DISCUSSION

Short-term hydroclimatic signal and hydrological context

The clearest association in the matched analysis occurred during the final 1–3 d before first satellite active-fire detection. Higher VPD indicates stronger atmospheric evaporative demand, while both rainfall anomaly and absolute rainfall accumulation indicate reduced water input over the same period; the accompanying increase in dry-day frequency provides a complementary expression of this deficit. Together, these findings are consistent with evidence from tropical peatlands linking drought and fire risk to rainfall and hydrological conditions (Taufik et al., 2022, 2023). Related modeling and field evidence likewise underscores the importance of hydrological controls on peat-fire occurrence (Mezbahuddin et al., 2023; Irfan et al., 2024). VPD has also been identified as an informative indicator of fire-favorable atmospheric demand across other biomes (Clarke et al., 2022; Jain et al., 2022). Recent work in the Himalayas provides further evidence that VPD can strongly constrain burned-area variability (Khadke and Ghosh, 2024). Because the VPD confidence interval was relatively wide, its magnitude should be interpreted cautiously; the stronger message is the timing of the association and its consistency across several indicators of short-term drying.

The multiplicity diagnostics favor a cautious interpretation of the lag-specific results as a temporally concentrated pattern rather than a collection of isolated significance tests. Adjustment across the five prespecified lag blocks attenuated conventional statistical significance for the individual 1–3-d estimates. However, shared-bootstrap contrasts showed that the positive VPD association and inverse rainfall association were stronger at 1–3 d than, on average, across the longer antecedent windows. The evidence therefore points to concentration near first detection while retaining appropriate uncertainty around any single lag-specific estimate.

Observation opportunity is central to this interpretation because t0 represents first satellite detection rather than ignition. Dates with more valid Terra, Aqua, and VIIRS observations provide more opportunities for an active-fire signal to be recorded, so the n_valid_sensors coefficient primarily reflects ascertainment rather than a physical driver of fire. Because this covariate is derived from the same product family used to define t0, it is not fully external to the outcome process. Importantly, the short-term VPD and rainfall estimates were similar when observation-opportunity adjustment was omitted, replaced with valid-land fraction, or restricted by excluding zero-opportunity referents, reducing concern that the main hydroclimatic pattern was created by this adjustment choice. The leave-one-year-out analysis likewise

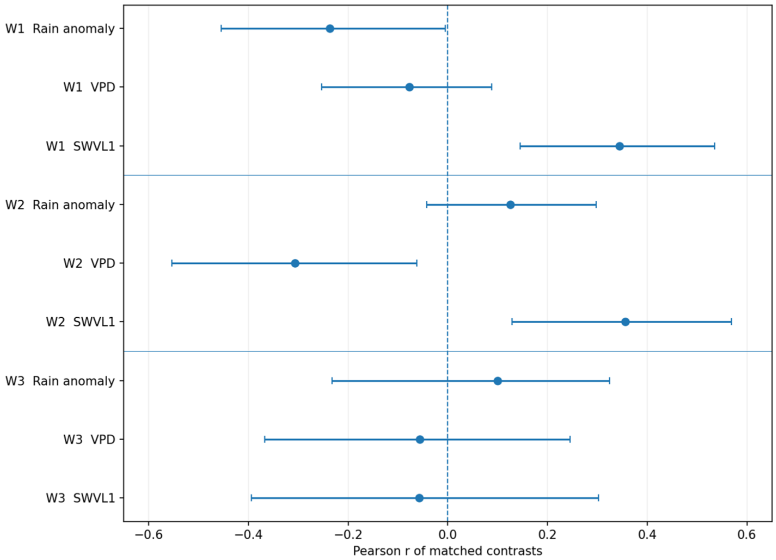

Figure 7. Sentinel-1–hydroclimate wetness concordance across temporally aligned antecedent windows
Note: Points represent Pearson correlations between case-minus-mean-referent ΔVV contrasts and the corresponding hydroclimatic contrasts, with error bars indicating 95% percentile intervals from 2000 stratum-level bootstrap replicates. W1, W2, and W3 represent 31–60, 15–30, and 1–14 d before the index date, respectively. ΔVV is interpreted as a moisture-sensitive indicator of surface conditions rather than as a direct measure of absolute soil moisture

Table 2. Selected primary and supporting association estimates

Indicator	Window	Estimate	Bootstrap 95% CI
Mean VPD	1–3 d	OR 4.07	1.43–13.54
Rainfall anomaly	1–3 d	OR 0.66	0.45–0.86
Rainfall accumulation	1–3 d	OR 0.42	0.22–0.65
Dry days (<1 mm)	1–3 d	OR 2.29	1.26–4.56
ΔVV after H-VPD	W1	OR 1.02	0.52–2.22
ΔVV–SWVL1 concordance	W1	r 0.34	0.14–0.53

preserved the direction of both primary associations. Excluding 2015, which contributed 49 of 79 events, substantially increased uncertainty but did not reverse the estimates. This does not remove the temporal imbalance; instead, it highlights the limited information available outside the dominant 2015 fire year and the resulting constraints on precision and generalizability.

ERA5-Land soil-water variables should be interpreted as hydrological context rather than direct measurements of peat water-table conditions. SWVL1 and SWVL2 were broadly consistent with drying, but their estimates were comparatively imprecise, and the strong within-stratum relationship between VPD and SWVL1 limits separation of their individual contributions. Field evidence also indicates that peat water-table depth and near-surface soil-water conditions can respond differently to rainfall, drainage, and restoration, reinforcing the need to avoid translating gridded soil-water products directly into groundwater-depth estimates (Treby et al., 2026). At the landscape scale, drainage structure and land cover remain important determinants of persistent peat-fire susceptibility (Salmayenti et al., 2025). The case-crossover design complements this spatial perspective by asking a different question: how conditions change within the same locations immediately before a fire is first detected from space.

Sentinel-1 as complementary wetness evidence

Sentinel-1 produced a more nuanced signal than the hydroclimatic variables. Although W1 had the greatest acquisition support, ΔVV remained close to the null after hydroclimatic adjustment and did not improve model fit. Similar results were obtained for W2, W3, B90, and the prior-event-clean sensitivity analyses. The concordance analysis nevertheless showed that ΔVV retained hydrologically relevant information: it was positively correlated with SWVL1 at W1 and W2 and inversely correlated with VPD at W2. These relationships are consistent with the moisture sensitivity of C-band backscatter, but their temporal variability and weaker correspondence with rainfall argue against interpreting ΔVV as a direct measure of soil moisture (Hrysiewicz et al., 2023; Pelletier et al., 2023).

A plausible interpretation is that Sentinel-1 captured aspects of surface wetness that overlapped with conditions represented by rainfall, atmospheric demand, and gridded soil-water variables. ΔVV may therefore provide useful complementary evidence of antecedent surface conditions without adding stable incremental information once those hydroclimatic variables are included in the model. This interpretation is consistent with peatland studies using Sentinel-1 backscatter as a surface-wetness or fire-vulnerability indicator (Hrysiewicz et al., 2023; Millard et al., 2022). Related remote-sensing work likewise supports the value of wetness-sensitive time-series information for peatland fire likelihood (Pelletier et al., 2023).

The prior-event audit further examined whether earlier fires might influence the radar signal. Excluding observations with antecedent overlap from earlier reconstructed events shifted some ΔVV estimates but reduced the matched sample and increased uncertainty. The lack of consistent improvement after this restriction suggests that earlier-event contamination alone is unlikely to explain the limited incremental contribution of ΔVV, while illustrating the trade-off between stricter temporal exclusion and statistical precision.

Implications for peat-fire monitoring

The findings support a monitoring framework rather than a deterministic fire threshold. Short-term hydroclimatic indicators – particularly VPD and recent rainfall – provided the clearest near-term information during the 1–3 d preceding first retained satellite detection. Sentinel-1 was more informative as a complementary indicator of antecedent surface wetness when suitable observations were available. This distinction matters operationally because hydroclimatic products provide more regular temporal coverage, whereas Sentinel-1 remains constrained by acquisition timing and quality-control requirements. Recent Indonesian studies similarly support combining fire-weather and drought indicators for peat-fire monitoring (Hayasaka, 2023; Lisnawati et al., 2022). Evidence from peatland rewetting further underscores the importance of hydrological controls on fire hazard (Taufik et al., 2023).

In practice, this framework could help identify periods warranting closer surveillance when atmospheric drying intensifies and recent rainfall declines. The present results, however, do not constitute a validated forecasting system. Prospective testing across additional peatland landscapes, regional calibration, integration of land-management and hydrological information, and better characterization of ignition timing are needed before operational warning thresholds or predictive performance can be established.

Limitations and generalizability

Several limitations constrain inference. First, t0 marks the first retained satellite detection rather than ignition, so all lag windows are anchored to observation and cannot resolve combustion onset. Second, the analysis was confined to a single 142.35-km² peatland landscape, and 49 of 79 events occurred in 2015. Although leave-one-year-out analyses preserved the direction of the primary associations, they cannot substitute for external validation across other peatland, management, and climatic settings. Third, the primary population included only non-singleton reconstructed events. This choice increases confidence that event units are supported by repeated detections but may underrepresent short-lived, low-intensity, or poorly observed fires; the findings therefore do not characterize the full spectrum of peat-fire episodes.

Fourth, CHIRPS and ERA5-Land are gridded products whose spatial resolutions are coarser than the event-scale extraction buffers. SWVL1 and SWVL2 were therefore interpreted as indicators of broader soil-water conditions rather than field measurements of peat groundwater or water-table depth. Sentinel-1 observations were temporally intermittent, and C-band backscatter can respond to vegetation, surface structure, hydrological conditions, and acquisition geometry as well as moisture (Hrysiewicz et al., 2023).

ΔVV should therefore be regarded as a moisture-sensitive indicator rather than a quantitative soil-moisture measure.

Fifth, n_valid_sensors was derived from the same active-fire product family used to define t0 and should be viewed as an ascertainment-process covariate, not a fully external predictor. The agreement of estimates under unadjusted, valid-land-fraction, and zero-opportunity-restricted analyses reduces but does not eliminate this concern. Sixth, supporting hydrological and wetness-concordance analyses were conducted after the primary framework had been fixed and were interpreted as complementary rather than confirmatory evidence. The zero-opportunity, archive-edge, and multiplicity analyses were likewise post hoc robustness diagnostics. Because the upstream response inventory begins on 22 February 2015, prior reconstructed-event history cannot be audited for the three earlier referents in STR_C0001; excluding that stratum did not materially change the primary estimates. Finally, although the time-stratified case-crossover design controls for time-invariant spatial characteristics and much of the seasonal background, residual time-varying confounding cannot be excluded.

These constraints limit the findings to relative, detection-anchored associations within the study landscape and argue against interpreting the estimates as ignition thresholds, causal effects, or a validated forecasting rule.

CONCLUSIONS

In this time-stratified case-crossover analysis of 79 reconstructed non-singleton peat-fire events, the clearest hydroclimatic signal was concentrated in the 1–3 d before first retained satellite active-fire detection. Higher VPD, an inverse association with wetter rainfall anomalies, lower rainfall accumulation, and more dry days formed a coherent short-term drying pattern. Gridded soil-water indicators were directionally consistent but less precise, and the direction of the main associations was stable across key sensitivity analyses.

Sentinel-1 ΔVV did not materially improve hydroclimatic model fit after adjustment for observation opportunity, although its positive concordance with SWVL1 during W1 and W2 supported its role as complementary evidence of antecedent surface wetness. Overall, the results support an observation-aware interpretation in which hydroclimatic indicators provide the clearest near-term information before first satellite detection, while Sentinel-1 contributes complementary wetness context.

Acknowledgements

The authors acknowledge the Doctoral Program in Environmental Science, Universitas Sriwijaya, for its academic and institutional support. The authors also thank NASA FIRMS for providing access to the active-fire datasets used in this study.

REFERENCES

1. Anda, M., Ritung, S., Suryani, E., Sukarman, Hikmat, M., Yatno, E., Mulyani, A., Subandiono, R. E., Suratman, Husnain. (2021). Revisiting tropical peatlands in Indonesia: Semi-detailed mapping, extent and depth distribution assessment. *Geoderma*, *402*, 115235. https://doi.org/10.1016/j.geoderma.2021.115235
2. Chen, Y., Hantson, S., Andela, N., Coffield, S. R., Graff, C. A., Morton, D. C., Ott, L. E., Foufoula-Georgiou, E., Smyth, P., Goulden, M. L., Randerson, J. T. (2022). California wildfire spread derived using VIIRS satellite observations and an object-based tracking system. *Scientific Data*, *9*, 249. https://doi.org/10.1038/s41597-022-01343-0
3. Clarke, H., Nolan, R. H., Resco de Dios, V., Bradstock, R., Griebel, A., Khanal, S., Boer, M. M. (2022). Forest fire threatens global carbon sinks and population centres under rising atmospheric water demand. *Nature Communications*, *13*, 7161. https://doi.org/10.1038/s41467-022-34966-3
4. Fitra, M. R., Suwignyo, R. A., Putranto, D. D. A., Mardiansyah, W. (2026a). Reconstructing MODIS/VIIRS candidate fire events in a tropical peatland landscape: Sentinel-1 corroboration, robustness, and independent Landsat audit [Data set]. *Zenodo*. https://doi.org/10.5281/zenodo.21876078
5. Fitra, M. R., Suwignyo, R. A., Putranto, D. D. A., Mardiansyah, W. (2026b). Short-term hydroclimatic precursors before the first satellite detection of peat-fire events in South Sumatra: An observation-aware case-crossover analysis (Version 1.0.0) [Data set]. *Zenodo*. https://doi.org/10.5281/zenodo.21899090
6. Funk, C., Peterson, P., Landsfeld, M., Pedreros, D., Verdin, J., Shukla, S., Husak, G., Rowland, J., Harrison, L., Hoell, A., Michaelsen, J. (2015). The climate hazards infrared precipitation with stations—a new environmental record for monitoring extremes. *Scientific Data*, *2*, 150066. https://doi.org/10.1038/sdata.2015.66
7. Giglio, L., Schroeder, W., Justice, C. O. (2016). The collection 6 MODIS active fire detection algorithm

and fire products. *Remote Sensing of Environment*, *178*, 31–41. https://doi.org/10.1016/j.rse.2016.02.054

8. Hayasaka, H. (2023). Peatland fire weather conditions in Sumatra, Indonesia. *Climate*, *11*(5), 92. https://doi.org/10.3390/cli11050092
9. Hrysiewicz, A., Holohan, E. P., Donohue, S., Cushnan, H. (2023). SAR and InSAR data linked to soil moisture changes on a temperate raised peatland subjected to a wildfire. *Remote Sensing of Environment*, *291*, 113516. https://doi.org/10.1016/j.rse.2023.113516
10. Irfan, M., Koriyanti, E., Saleh, K., Hadi, Safrina, S., Awaludin, Sulaiman, A., Akhsan, H., Suhadi, Suwignyo, R. A., Choi, E., Iskandar, I. (2024). Dynamics of peatland fires in South Sumatra in 2019: Role of groundwater levels. *Land*, *13*(3), 373. https://doi.org/10.3390/land13030373
11. Jain, P., Castellanos-Acuna, D., Coogan, S. C. P., Abatzoglou, J. T., Flannigan, M. D. (2022). Observed increases in extreme fire weather driven by atmospheric humidity and temperature. *Nature Climate Change*, *12*, 63–70. https://doi.org/10.1038/s41558-021-01224-1
12. Khadke, L., Ghosh, S. (2024). Vapor pressure deficit controls the extent of burned area over the Himalayas. *Journal of Geophysical Research: Atmospheres*, *129*(22), e2024JD041155. https://doi.org/10.1029/2024JD041155
13. Lisnawati, Taufik, M., Dasanto, B. D., Sopaheluwakan, A. (2022). Fire danger on Jambi peatland, Indonesia, based on the Weather Research and Forecasting model. *Agromet*, *36*(1), 1–10. https://doi.org/10.29244/j.agromet.36.1.1-10
14. McClure, C. D., Pavlovic, N. R., Huang, S. M., Chaveste, M., Wang, N. (2023). Consistent, high-accuracy mapping of daily and sub-daily wildfire growth with satellite observations. *International Journal of Wildland Fire*, *32*(5), 694–708. https://doi.org/10.1071/WF22048
15. Mezbahuddin, S., Nikonovas, T., Spessa, A., Grant, R. F., Imron, M. A., Doerr, S. H., Clay, G. D. (2023). Accuracy of tropical peat and non-peat fire forecasts enhanced by simulating hydrology. *Scientific Reports*, *13*, 619. https://doi.org/10.1038/s41598-022-27075-0
16. Millard, K., Darling, S., Pelletier, N., Schultz, S. (2022). Seasonally-decomposed Sentinel-1 backscatter time-series are useful indicators of peatland wildfire vulnerability. *Remote Sensing of Environment*, *283*, 113329. https://doi.org/10.1016/j.rse.2022.113329
17. Mullissa, A., Vollrath, A., Odongo-Braun, C., Slagter, B., Balling, J., Gou, Y., Gorelick, N., Reiche, J. (2021). Sentinel-1 SAR backscatter analysis ready data preparation in Google Earth Engine. *Remote Sensing*, *13*(10), 1954. https://doi.org/10.3390/rs13101954
18. Muñoz-Sabater, J., Dutra, E., Agustí-Panareda, A., Albergel, C., Arduini, G., Balsamo, G., Boussetta, S., Choulga, M., Harrigan, S., Hersbach, H., Martens, B., Miralles, D. G., Piles, M., Rodríguez-Fernández, N. J., Zsoter, E., Buontempo, C., Thépaut, J.-N. (2021). ERA5-Land: A state-of-the-art global reanalysis dataset for land applications. *Earth System Science Data*, *13*, 4349–4383. https://doi.org/10.5194/essd-13-4349-2021
19. Pelletier, N., Millard, K., Darling, S. (2023). Wildfire likelihood in Canadian treed peatlands based on remote-sensing time-series of surface conditions. *Remote Sensing of Environment*, *296*, 113747. https://doi.org/10.1016/j.rse.2023.113747
20. Quast, R., Wagner, W., Bauer-Marschallinger, B., Vreugdenhil, M. (2023). Soil moisture retrieval from Sentinel-1 using a first-order radiative transfer model—A case-study over the Po-Valley. *Remote Sensing of Environment*, *295*, 113651. https://doi.org/10.1016/j.rse.2023.113651
21. Salmayenti, R., Baird, A. J., Holden, J., Spracklen, D. V. (2025). Drainage density and land cover interact to affect fire occurrence in Indonesian peatlands. *Environmental Research Letters*, *20*(5), 054036. https://doi.org/10.1088/1748-9326/adc755
22. Schroeder, W., Oliva, P., Giglio, L., Csiszar, I. A. (2014). The new VIIRS 375 m active fire detection data product: Algorithm description and initial assessment. *Remote Sensing of Environment*, *143*, 85–96. https://doi.org/10.1016/j.rse.2013.12.008
23. Taufik, M., Widyastuti, M. T., Sulaiman, A., Murdiyarso, D., Santikayasa, I. P., Minasny, B. (2022). An improved drought-fire assessment for managing fire risks in tropical peatlands. *Agricultural and Forest Meteorology*, *312*, 108738. https://doi.org/10.1016/j.agrformet.2021.108738
24. Taufik, M., Haikal, M., Widyastuti, M. T., Arif, C., Santikayasa, I. P. (2023). The impact of rewetting peatland on fire hazard in Riau, Indonesia. *Sustainability*, *15*(3), 2169. https://doi.org/10.3390/su15032169
25. Tobias, A., Kim, Y., Madaniyazi, L. (2024). Time-stratified case-crossover studies for aggregated data in environmental epidemiology: A tutorial. *International Journal of Epidemiology*, *53*(2), dyae020. https://doi.org/10.1093/ije/dyae020
26. Torres, R., Snoeij, P., Geudtner, D., Bibby, D., Davidson, M., Attema, E., Potin, P., Rommen, B., Floury, N., Brown, M., Traver, I. N., Deghaye, P., Duesmann, B., Rosich, B., Miranda, N., Bruno, C., L'Abbate, M., Croci, R., Pietropaolo, A.,... Rostan, F. (2012). GMES Sentinel-1 mission. *Remote Sensing of Environment*, *120*, 9–24. https://doi.org/10.1016/j.rse.2011.05.028
27. Treby, S., Graham, L. L. B., Ningsih, S. N. A., Thomas, A., Grover, S. P. P. (2026). Soil hydrology in a drained tropical peatland in Central Kalimantan, Indonesia: Implications for land management. *Pedosphere*. Advance online publication. https://doi.org/10.1016/j.pedsph.2026.02.009